© 2015. Published by The Company of Biologists Ltd | Development (2015) 142, 162-173 doi:10.1242/dev.113423

RESEARCH ARTICLE

Coordinate control of terminal dendrite patterning and dynamics by the membrane protein Raw

Jiae Lee, Yun Peng, Wen-Yang Lin and Jay Z. Parrish*

ABSTRACT

The directional flow of information in neurons depends on compartmentalization: dendrites receive inputs whereas axons transmit them. Axons and dendrites likewise contain structurally and functionally distinct subcompartments. Axon/dendrite compartmentalization can be attributed to neuronal polarization, but the developmental origin of subcompartments in axons and dendrites is less well understood. To identify the developmental bases for compartment-specific patterning in dendrites, we screened for mutations that affect discrete dendritic domains in *Drosophila* sensory neurons. From this screen, we identified mutations that affected distinct aspects of terminal dendrite development with little or no effect on major dendrite patterning. Mutation of one gene, *raw*, affected multiple aspects of terminal dendrite patterning, suggesting that Raw might coordinate multiple signaling pathways to shape terminal dendrite growth. Consistent with this notion, Raw localizes to branch-points and promotes dendrite stabilization together with the Tricornered (Trc) kinase via effects on cell adhesion. Raw independently influences terminal dendrite elongation through a mechanism that involves modulation of the cytoskeleton, and this pathway is likely to involve the RNA-binding protein Argonaute 1 (AGO1), as *raw* and *AGO1* genetically interact to promote terminal dendrite growth but not adhesion. Thus, Raw defines a potential point of convergence in distinct pathways shaping terminal dendrite patterning.

KEY WORDS: Dendrite, Compartmentalization, Terminal dendrite dynamics

INTRODUCTION

The directional flow of information in the nervous system relies on the compartmentalization of neurons. On a basic level, a neuron has two compartments apart from the soma: dendrites, which receive inputs, and axons, which transmit signals. To meet their respective functions, axons and dendrites have distinct morphological and molecular properties. For example, the microtubule cytoskeleton is organized differently in axons and dendrites, allowing distinct modes of trafficking (Baas et al., 1988; Horton and Ehlers, 2003). Beyond this basic level of compartmentalization, neurons display extreme diversity in axon and dendrite morphology, and both axons and dendrites contain structurally and functionally distinct subdomains (Katsuki et al., 2011; Masland, 2004).

Several lines of evidence support the existence of compartments within dendrites. First, some neurons have morphologically distinct dendrites. For example, mammalian olfactory bulb mitral cells extend a tufted primary dendrite radially and structurally and functionally distinct lateral dendrites horizontally (Imamura and Greer, 2009). Likewise, apical/basal dendrites of hippocampal neurons and ipsilateral/contralateral dendrites of motoneurons are morphologically and biophysically distinct. Second, specialized structures are asymmetrically distributed in many dendrites. Notable among these is the dendritic spine, an isolated compartment that is electrically and biochemically distinct from the rest of the dendrite arbor, and dendritic spines likewise have distinctive microdomains (Chen and Sabatini, 2012; Yuste, 2013). Many organelles are selectively deployed in dendrites, including a satellite secretory pathway containing endoplasmic reticulum and Golgi outposts; the number and location of these organelles locally influences dendrite growth and dynamics (Aridor et al., 2004; Gardiol et al., 1999; Horton and Ehlers, 2003; Ye et al., 2007). In highly branched dendrite arbors, for example cerebellar Purkinje neurons and insect sensory neurons, major dendrites and terminal dendrites have distinct cytoskeletal compositions and growth properties (Fujishima et al., 2012; Jinushi-Nakao et al., 2007). Finally, dendrite arbors often contain functionally distinct domains as well. For example, the proximal-distal compartmentalization of chloride co-transporters underlies directional selectivity in starburst amacrine cells (Gavrikov et al., 2006). Whereas axon/dendrite compartmentalization can be attributed to neuronal polarization, the developmental origin of dendrite subcompartments is less well understood.

Drosophila peripheral nervous system (PNS) class IV dendrite arborization (C4da) neurons have highly branched dendrite arbors, consisting of major dendrites emanating radially from the soma and terminal dendrites that fill in the space in the receptive field (Grueber et al., 2002). Main branches and terminal arbors have distinct growth properties in these neurons, with terminal dendrites exhibiting dynamic growth and containing a cytoskeleton largely devoid of microtubules (Grueber et al., 2002; Jinushi-Nakao et al., 2007), suggesting that different cellular programs pattern main dendrites and terminal arbors. To identify the developmental bases for compartment-specific patterning in these dendrites, we used a genetic screen to identify mutations that affect distinct dendritic compartments. From this screen, we identified mutants that selectively affected terminal dendrites, including their placement along the proximal-distal axis and their patterning, suggesting that distance from the soma and branch type (major or terminal dendrite) are two key pieces of positional information in the patterning of dendrite arbors. Mutations in *raw* were unique in that they simultaneously affected multiple aspects of terminal dendrite patterning, suggesting that *raw* coordinately controls multiple aspects of terminal dendrite growth. Indeed, we found that Raw regulates terminal dendrite adhesion and elongation via distinct pathways, the former involving the Trc kinase and the latter involving cytoskeletal remodeling and the RNA-binding protein AGO1. Thus, Raw appears to be a crucial component of a spatially localized program controlling terminal dendrite patterning.

Department of Biology, University of Washington, Seattle, WA 98195, USA.

*Author for correspondence (jzp2@uw.edu)

Received 28 May 2014; Accepted 31 October 2014

Development (2015) 142, 162-173 doi:10.1242/dev.113423

RESULTS

Identification of mutations that affect dendrite compartmentalization

To identify the developmental bases for compartment-specific patterning in dendrites, we used mosaic analysis with a repressible cell marker (MARCM) to screen for mutations that differentially affected different regions of C4da dendrite arbors (Lee and Luo, 1999). From this screen, we identified two phenotypic groups that define different levels of organization of these dendrite arbors. First, we identified mutations that differentially affected terminal dendrite growth/distribution along a proximal-distal axis relative to the cell body (supplementary material Fig. S1). Most commonly, as in *jj329* mutant neurons, mutants in this group caused exuberant terminal dendrite branching in proximity to the soma and reduced terminal branching distally (supplementary material Fig. S1). Notably, this phenotype is similar to dendrite phenotypes caused by mutations in *Dlic* (Satoh et al., 2008; Zheng et al., 2008), and thus we hypothesize that organization along the proximal-distal axis involves spatial information conferred by microtubule-based transport. Consistent with this hypothesis, *jj329* is an allele of *CG12042*, which encodes Dynactin subunit 4, and several other mutants in this group impinge on microtubule-based processes. Second, we identified a large group of mutants that preferentially affect terminal dendrite patterning without affecting major dendrites. Within this group, we identified mutants that affected the number, length and/or orientation of terminal dendrites. For example, *jj472* had simplified terminal arbors; *jj835* mutants were devoid of higher order branches; and *jj599* mutants affected terminal dendrite self-avoidance (supplementary material Fig. S1). The identification of mutants that show deficits in the formation of terminal dendrite arbors (*jj835*) and distinct aspects of terminal patterning (length, *jj472*; avoidance, *jj599*) suggests that multiple pathways function at different levels of control to pattern terminal dendrites.

We anticipated that we would identify mutations that selectively affect primary dendrite growth; however, we have not identified any such mutations, possibly indicating that primary dendrite growth is a prerequisite for terminal dendrite branching in these neurons (Parrish et al., 2006). Nevertheless, results from our screen suggest that dendrite arbor development in C4da neurons is compartmentalized in at least two ways: growth of terminal dendrites along a proximal-distal axis emanating from the cell body, and in patterning of main and terminal dendrites.

raw regulates multiple aspects of terminal dendrite patterning

Among the mutants that preferentially affected terminal dendrites, *jj102* was of particular interest because it affected multiple aspects of terminal dendrite patterning, suggesting that it might coordinately regulate multiple signaling pathways that influence terminal dendrites (Fig. 1). *jj102* mutant C4da neurons exhibited four characteristic terminal dendrite defects. First, major dendrites were decorated with short, mostly unbranched terminal dendrites, whereas major dendrites in control neurons had extensively branched terminal arbors. Thus, although the total branch number and distribution along the proximal-distal axis were comparable in *jj102* mutants and wild-type controls (Fig. 1E, left; supplementary material Fig. S2A), *jj102* mutant neurons exhibited reduced complexity in distal regions of the arbor, which normally contain highly branched dendrites (Fig. 1E, middle and right). Consequently, the average path length from soma to dendrite tip was significantly shorter in *jj102* mutants (Fig. 1F). Second, the average terminal dendrite length was significantly reduced in *jj102* mutants (Fig. 1G); consequently, total dendrite length was also reduced (supplementary material Fig. S2B). Third, terminal dendrite orientation was altered: both the local branch angle and three-dimensional (3D) placement of terminal dendrites were defective in *jj102* mutants. In wild-type neurons, branch angles of terminal dendrites approached 90°, contributing to the radial arrangement of dendrite arbors, but terminal dendrites of *jj102* mutants branched at more acute angles (Fig. 1H). As a result, terminal dendrites often grew in proximity to primary dendrites, rather than growing away from them. Fourth, dendrite-dendrite crossing events were common in *jj102* mutant neurons; whereas dendrites of wild-type neurons are confined to a two-dimensional (2D) area and rarely cross over one another (Fig. 1A′) (Emoto et al., 2004; Han et al., 2012; Kim et al., 2012), terminal dendrites in *raw* mutant neurons occupy larger 3D areas and frequently cross over one another (Fig. 1B′,I). Thus, *jj102* defines a potential point of convergence for the developmental control of multiple aspects of terminal dendrite patterning.

Homozygous *jj102* mutants arrest as embryos with dorsal closure defects, and *jj102* mapped to an interval on chromosome 2 containing one known regulator of dorsal closure, *raw* (Nusslein-Volhard et al., 1984). *raw* encodes a novel protein that modulates cell-cell signaling in dorsal closure (Bates et al., 2008; Bauer Huang et al., 2007; Byars et al., 1999) and Cadherin-based interactions between somatic gonadal precursor cells and germ cells (Jemc et al., 2012). Consistent with *jj102* affecting *raw* function, chromosome deficiencies that span *raw* and *raw* reduction-of-function alleles (raw^{1}, raw^{k01021}) failed to complement *jj102* lethality. Further, an independently derived *raw* allele (raw^{k01021}) phenocopied the *jj102* dendrite defects (Fig. 1C,F-I). Finally, *jj102* carries a nonsense mutation in *raw* (CAA→TAA, Q777Stop in Raw-short), which should lead to a premature stop prior to a predicted transmembrane domain (Fig. 1J) (Jones et al., 1994).

To establish that *jj102* dendrite defects were caused by loss of *raw* function, we used MARCM to resupply functional *raw* to *jj102* mutant neurons. To this end, we generated a transgene encoding a GFP-Raw fusion protein (*UAS-GFP-raw*, Fig. 1J) using the short isoform of *raw*, which has been implicated in PNS development (Prokopenko et al., 2000). *UAS-GFP-raw* fully rescued the *jj102* dendrite defects (Fig. 1D,F-I). By contrast, overexpressing *UAS-GFP-raw* in wild-type C4da neurons had no effect on terminal branch patterning (data not shown), and thus *raw* is necessary for terminal dendrite patterning but not sufficient to promote exuberant growth. Altogether, these results demonstrate that *raw* functions cell-autonomously to regulate terminal dendrite orientation and elongation, and that Raw-short can support dendrite development; we have not investigated the function of other isoforms in the PNS.

Raw promotes terminal dendrite stabilization

Homozygous *raw* mutants arrest before PNS dendrite outgrowth begins and *raw* influences the development of several embryonic tissues (Byars et al., 1999; Jack and Myette, 1997; Jemc et al., 2012; Kania et al., 1995). Therefore, to ascertain the developmental origin of the *raw* mutant dendrite defects, we monitored dendrite phenotypes of *raw* mutant MARCM clones during early larval development. At each stage that we observed (clones become visible in late first instar larvae), *raw* mutant neurons exhibited characteristic terminal branching defects while major dendrites grew comparably to controls (supplementary material Fig. S2). Thus, *raw* is required for dendrite development from early stages of larval development and appears to act primarily on terminal dendrites.

Development (2015) 142, 162-173 doi:10.1242/dev.113423

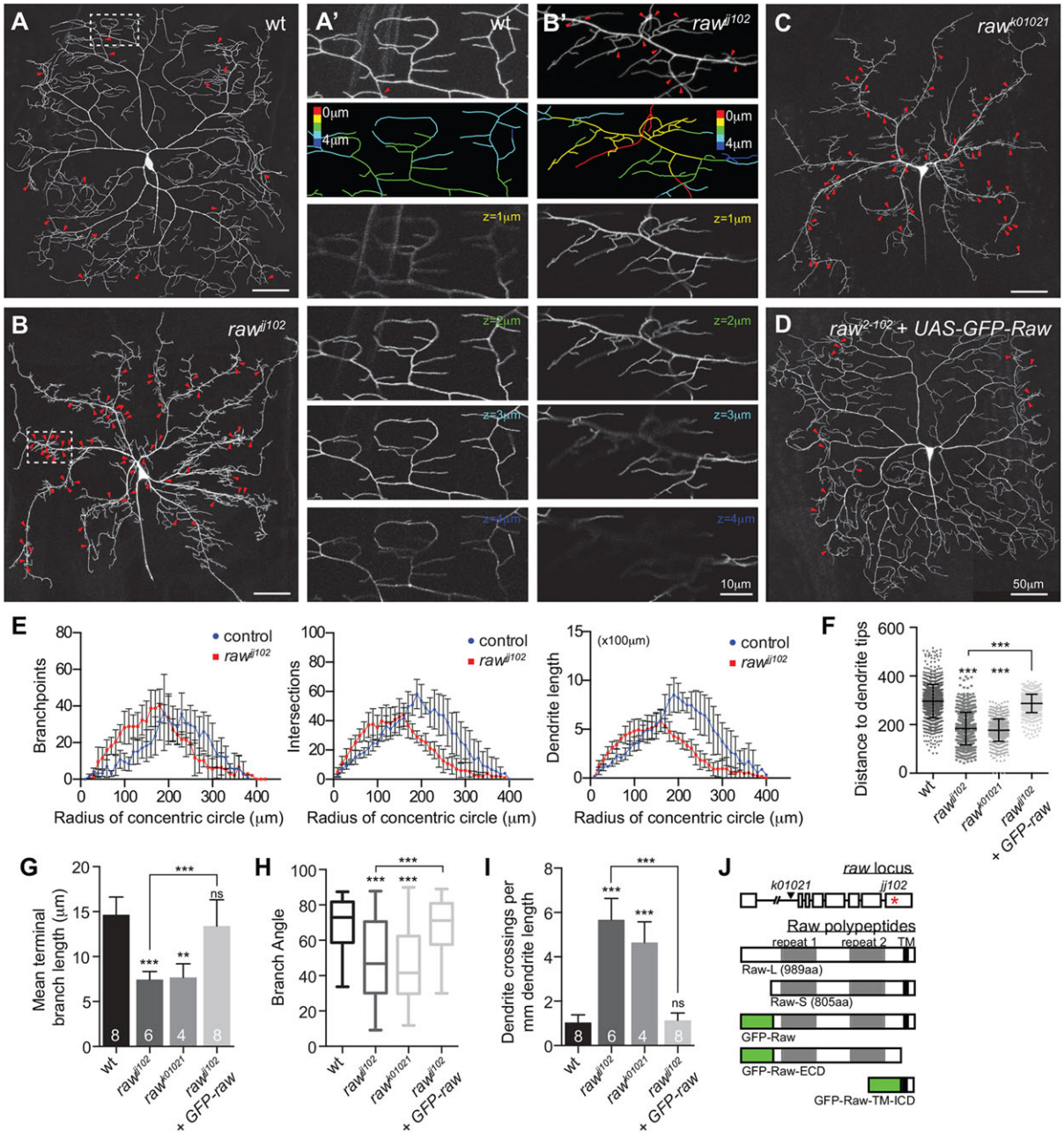

Fig. 1. Raw affects terminal dendrite patterning. Representative MARCM clones for wild-type (wt) control (A), *raw*^{ji102} (B), *raw*^{k01021} (C) and *raw*^{ji102}+*UAS-GFP-raw* (D). Arrowheads mark dendrite-dendrite crossings. The boxed regions of the control and *raw*^{ji102} are magnified in A′ and B′, respectively, to show the axial position of terminal dendrites. (E-I) Morphometric analysis of dendrites from C4da MARCM clones of the indicated genotypes. (E) Sholl analysis depicting the distribution of branch-points, intersections and dendrite length. (F) Scatter plot showing path lengths from the cell body to branch endings. Data points reflect measurements from a representative neuron; error bars indicate aggregate mean and 95% confidence interval (*n=8* for wt, 6 for *jj102*). (G) Average terminal branch length; error bars indicate s.d. (H) Terminal branch angles; box plots depict mean values and first/third quartile, whiskers mark minimum/maximum values. (I) Dendrite-dendrite crossing, normalized to total dendrite length. Error bars indicate s.d.; ns, not significant; ***P*<0.01, ****P*<0.001, relative to control; one-way ANOVA with post-hoc Dunnett's test. The number of neurons analyzed for each genotype is indicated in (I), and branch angles for 100 terminal dendrites were measured for each neuron in (H). Scale bars: 50 μm, except 10 μm for A′,B′. (J) Schematic of the *raw* locus, predicted polypeptides, and *GFP-raw* constructs. *k01021* carries a *P{lacW}* insertion, and *jj102* carries a missense mutation (red asterisk) in the last coding exon. Raw has two ~100 amino acid repeats of unknown function and a putative C-terminal transmembrane domain (TM). Raw-L, Raw-long; Raw-S, Raw-short; ECD, extracellular domain; ICD, intracellular domain.

The *raw* mutant dendrite branching defects could reflect a failure in terminal branch elongation, increased branch retraction, or some combination of both. To distinguish between these possibilities, we monitored terminal dendrite dynamics in wild-type or *raw* mutant C4da MARCM clones using time-lapse microscopy. Initially, we chose a 4-h window beginning at 96 h after egg laying (AEL), when larval growth is nearly complete and C4da dendrite arbors are no longer expanding (Parrish et al., 2009). During this time-lapse most terminal dendrites exhibit dynamics with equivalent rates of branch extension and retraction (Fig. 2A,C,D). By contrast, a significantly larger proportion of terminals exhibited dynamics in *raw* mutant neurons, with dynamic branches retracting more frequently than they grew (Fig. 2B-D). Additionally, the extent of dynamics was significantly increased in *raw* mutants (3.8 μm on average,

Development (2015) 142, 162-173 doi:10.1242/dev.113423

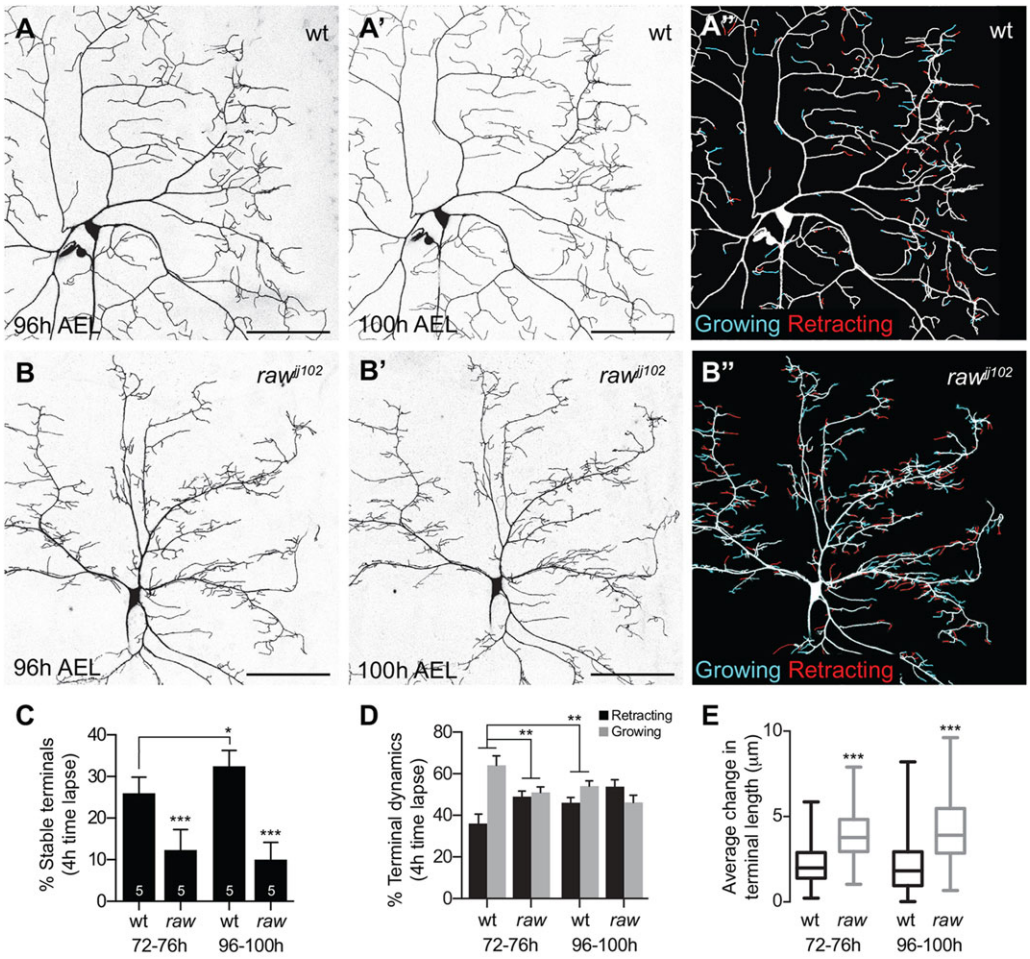

Fig. 2. Raw regulates terminal branch dynamics. (A-B″) Time-lapse analysis of terminal dendrite dynamics in wild-type (A-A″) and *raw*^{ij102} (B-B″) ddaC MARCM clones imaged at 96 h (A,B) and 100 h (A′,B′) AEL. (A″,B″) Growth (cyan) and retraction (red) are pseudocolored in a composite of the two time points. (C-E) Quantification of terminal dendrite dynamics (72-76 h or 96-100 h AEL) in wild-type and *raw*^{ij102} MARCM clones. *n*=5 neurons for each genotype. Dynamics were measured for at least 100 terminal dendrites in each neuron. The proportion of (C) stable and (D) dynamic terminals is shown. Error bars indicate s.d. (E) Change in terminal dendrite length for dynamic terminals. Box plots depict mean values and first/third quartile; whiskers mark minimum/maximum values. **P*<0.05, ***P*<0.01, ****P*<0.001; ns, not significant; one-way ANOVA with post-hoc Dunnett's test in C and E, binomial test in D. Scale bars: 100 μm.

compared with 1.8 μm for control neurons) (Fig. 2E). Thus, *raw* appears to regulate terminal dendrite stability.

Our developmental analysis of *raw* mutant neurons suggested that it is required for the stabilization of terminal branches throughout development. We therefore monitored dendrite dynamics over an earlier time-lapse when arbors are growing rapidly and adding new terminal dendrites. Between 72 and 76 h AEL, control neurons exhibited an increased frequency and a different distribution of dynamics: terminal growth occurred almost twice as frequently as retraction during the early interval, whereas growth and retraction occurred at equivalent rates during the late interval (Fig. 2C,D). As in the late time-lapse, *raw* mutants exhibited significantly more dynamic behavior than wild-type controls between 72 and 76 h AEL (Fig. 2C). Notably, whereas the dynamic behavior of control neurons changed during development, the rate of dynamics and the frequency of growth/retraction in *raw* mutant clones remained similar throughout both time-lapses, suggesting that terminal dendrite growth is constantly offset by retraction in *raw* mutants (Fig. 2D). Thus, *raw* affects terminal branch stability; at each time point examined, terminal dendrites of *raw* mutants were more dynamic than those of controls, with growth matched by retraction. Hence, terminal dendrites of *raw* mutants rarely branch or elongate, preventing the elaboration of terminal arbors.

Raw may function locally in dendrites to regulate terminal dendrite patterning

To gain insight into Raw control of terminal dendrite dynamics, we monitored the intracellular distribution of GFP-Raw in *raw* mutant C4da neuron clones. GFP-Raw rescues the *raw*^{ij102} dendrite defects, and thus we reasoned that GFP-Raw localization in these clones is likely to reflect the site of action of Raw. In dendrites, GFP-Raw is concentrated in puncta, most of which localize to branch-points along major dendrites (Fig. 3A, green arrowheads), consistent with Raw locally regulating terminal dendrite patterning. However, GFP-Raw was rarely detected in terminal dendrites, suggesting that Raw might function at branch-points to stabilize nascent dendrites or recruit other factors that function in the terminals.

Terminal dendrites rapidly turn over in *raw* mutants; therefore, we monitored whether GFP-Raw localization correlated with terminal branch stabilization. Using time-lapse microscopy, we monitored dendrite dynamics during an 18-h interval in GFP-Raw-expressing *raw*^{ij102} mutant C4da MARCM clones and examined whether the presence of GFP-Raw puncta at branch-points was associated with branch stabilization (Fig. 3B). We sampled over 500 dynamic terminal dendrites from six neurons and found that the growth behavior of terminal dendrites originating in branch-points containing GFP-Raw puncta [χ^2=23.80, degrees of freedom (d.f.)=2, *P*<0.01] or lacking GFP-Raw puncta (χ^2=14.90, d.f.=2, *P*<0.01) was significantly different from that of the population of terminal dendrites as a whole. Specifically, branches associated with GFP-Raw puncta were more likely to grow or remain the same length and less likely to retract, whereas branches emanating from branch-points lacking GFP-Raw were more likely to retract, consistent with Raw promoting terminal dendrite stabilization/elongation or marking stabilized terminals (Fig. 3C).

raw encodes a protein with a putative C-terminal transmembrane domain (Jones et al., 1994), and thus *raw* might encode a membrane

Development (2015) 142, 162-173 doi:10.1242/dev.113423

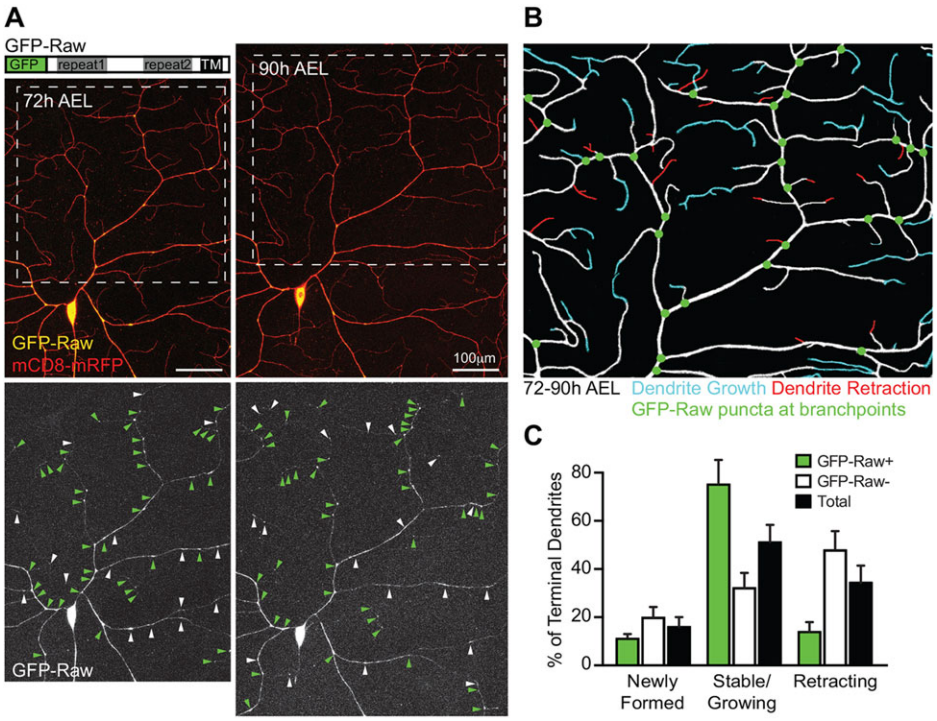

Fig. 3. Raw accumulates at branch-points of persistent dendrites. (A) Time-lapse imaging of *raw*^{ji102} C4da neuron MARCM clone expressing *UAS-GFP-raw* (structure illustrated at top), which rescues *raw*^{ji102} dendrite defects. The same neuron is imaged at 72 h and 90 h AEL. (Top row) Merge of GFP-Raw (yellow) and membrane-targeted mRFP (mCD8-mRFP; red) signals. (Bottom row) GFP-Raw distribution. Arrowheads mark GFP-Raw puncta: green, branch-point-localized puncta; white, puncta in interstitial regions. (B) Trace of region of interest (box in A) depicting dynamic terminal dendrites (red, retracting; cyan, growing) and GFP-Raw puncta localized at branch-points (green). 3/18 retracting terminals emanate from GFP-Raw-containing branch-points. (C) Quantification of dynamics for terminal dendrites emanating from branch-points containing GFP-Raw puncta (green), branch-points lacking GFP-Raw puncta (white), or all branch-points (black). *n*=6 clones; ~100 terminals were scored in each clone. Error bars indicate s.d.

protein that coordinately regulates multiple aspects of terminal dendrite development in response to extracellular cues. We therefore investigated whether Raw is membrane associated. We fractionated *Drosophila* S2 cells expressing GFP-Raw and probed the cellular fractions with antibodies to GFP, α-Tubulin (cytoplasmic marker) and Robo (membrane marker). Indeed, GFP-Raw was present in the cytoplasmic and membrane fractions, demonstrating that some of the GFP-Raw was membrane associated (Fig. 4A). Similarly, the *C. elegans* Raw ortholog (OLRN-1) is membrane associated, but OLRN-1 has multiple putative transmembrane domains that are not present in Raw (Bauer Huang et al., 2007).

Our membrane topology prediction suggested that the N-terminal ~700 amino acids of Raw constitute an extracellular domain (ECD), whereas the short C-terminus is located intracellularly (Jones et al., 1994). We therefore examined Raw distribution and topology using surface staining of 'rescued' *raw* mutant MARCM clones expressing GFP-Raw, reasoning that GFP should be surface exposed if Raw is targeted to the plasma membrane. As a negative control, we first assayed for surface-exposed GFP in MARCM clones expressing EB1-GFP, a microtubule-associated protein that should not be surface exposed. Although EB1-GFP was dispersed throughout the dendrite arbor, no GFP surface staining was evident, demonstrating that the plasma membrane was not permeabilized by our staining protocol (Fig. 4B). By contrast, C4da neurons expressing GFP-Raw exhibited punctate GFP surface staining (Fig. 4C), and these puncta frequently occurred at dendrite branch-points (green arrowheads). Similarly, GFP was surface exposed in S2 cells expressing GFP-Raw (data not shown). We conclude that Raw can associate with membranes and that the N-terminal domain can be exposed to the extracellular environment, with the potential to locally influence terminal dendrite development in response to extracellular cues.

raw interacts with the *trc* pathway to regulate terminal dendrite adhesion

We next set out to characterize downstream pathways by which Raw regulates terminal dendrite patterning. In dorsal closure and gonadal ensheathment, *raw* negatively regulates Jnk signaling to modulate cell-cell interactions (Byars et al., 1999; Jemc et al., 2012). We hypothesized that *raw* similarly regulates Jnk signaling in C4da neurons to pattern terminal dendrites. We therefore monitored effects of *raw* on phospho-Jnk accumulation, on expression of the Jnk pathway target *puckered*, and on AP-1 reporter expression in C4da neurons (Chatterjee and Bohmann, 2012), and in each case we observed no effect (supplementary material Fig. S3). Likewise, modulating Jnk activity had no apparent effect on C4da dendrite patterning. We therefore conclude that *raw* is likely to signal through distinct pathways in the epidermis and C4da neurons, with *raw* function in dendrite patterning being largely independent of Jnk signaling.

To identify genes that function with *raw* to regulate terminal dendrite patterning, we assayed for genetic interactions between *raw* and known regulators of terminal dendrite development, including genes in the Trc signaling pathway, that regulate dendrite-dendrite repulsion and terminal dendrite adhesion: *turtle* (*tutl*), which regulates dendrite-dendrite repulsion; *Dscam*, which regulates dendrite self-avoidance; and *myospheroid* (*mys*), which is required for dendrite-extracellular matrix (ECM) interactions (Emoto et al., 2004; Han et al., 2012; Kim et al., 2012; Koike-Kumagai et al., 2009; Long et al., 2009; Matthews et al., 2007; Soba et al., 2007). On its own, heterozygosity for mutation in *raw* or any of the other genes had no significant effect on the number of terminal dendrite crossing events, but larvae doubly heterozygous for mutations in *raw* and Trc signaling pathway genes exhibited significant increases in dendrite-dendrite crossing (Fig. 5), suggesting that Raw functions together with the Trc pathway to regulate terminal dendrite patterning. Similar to *raw*, *trc* regulates multiple aspects of terminal dendrite patterning, namely terminal dendrite number and adhesion, and these activities are genetically separable (Emoto et al., 2004). However, we observed significant changes in dendrite-dendrite crossing but not dendrite number in *raw trc* double heterozygotes, suggesting that the different functions of *raw* in terminal branching are likewise genetically separable, with terminal dendrite adhesion involving *trc*.

Development (2015) 142, 162-173 doi:10.1242/dev.113423

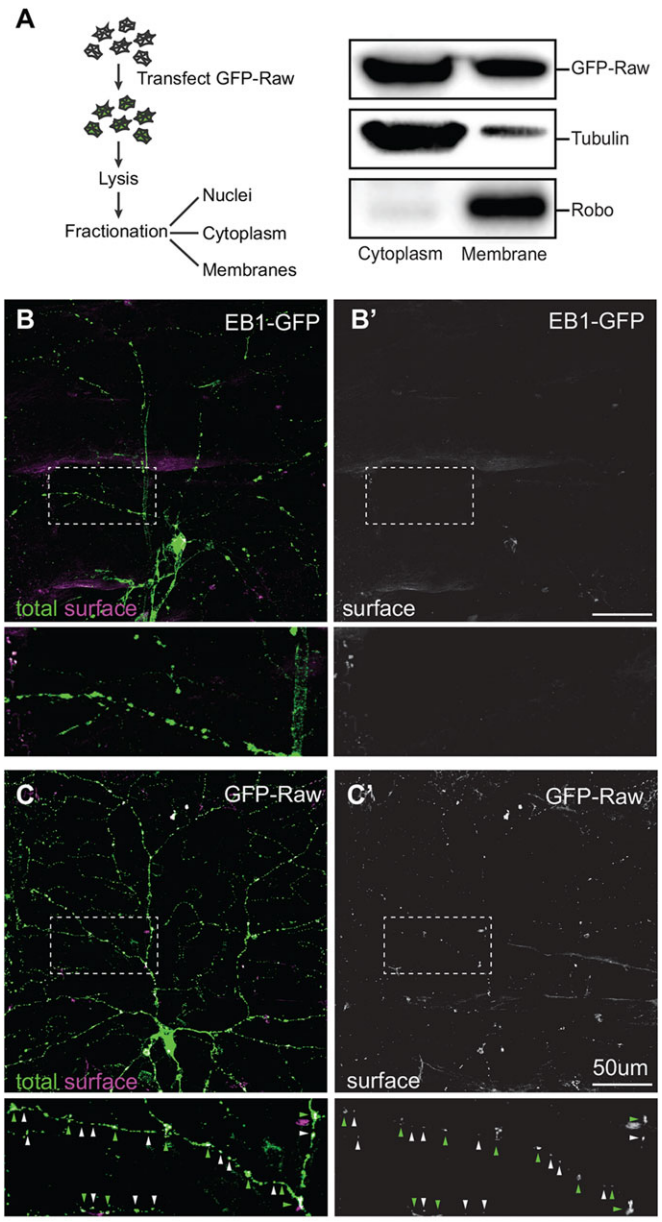

Fig. 4. Raw localizes to the plasma membrane. (A) Raw associates with membranes in *Drosophila* S2 cells. (Left) Cell fractionation workflow. (Right) Western blot of cytoplasm and membrane fractions probed with GFP (GFP-Raw), Tubulin (cytoplasm) and Robo (membrane) antibodies. (B-C′) GFP-Raw localizes to the dendritic plasma membrane. Total GFP fluorescence after fixation (B) and surface-exposed GFP revealed by immunostaining under non-permeabilizing conditions (B′) for a wild-type C4da MARCM clone expressing *UAS-EB1-GFP*. Total GFP fluorescence after fixation (C) and surface-exposed GFP-Raw (C′) for a raw^{j102} C4da neuron MARCM clone expressing *UAS-GFP-raw*. Boxed regions are magnified beneath. Arrowheads indicate GFP-Raw puncta: green arrowheads, puncta at branch-points; white arrowheads, additional GFP-Raw puncta. Additional puncta are likely to localize to branch-points, but we cannot unambiguously identify all branch-points with this fixation protocol. Scale bars: 50 µm.

Next, we assayed for physical association between Raw and Trc. We co-expressed GFP-Raw and Trc-mCherry-HA in S2 cells and examined whether the epitope-tagged proteins co-immunoprecipitated. Indeed, Raw co-immunoprecipitated with Trc and vice versa (Fig. 6A), and a truncated Raw protein containing the transmembrane domain and intracellular domain (TM-ICD) interacted with Trc, whereas the Raw ECD did not (Fig. 6B). Trc activation is potentiated by membrane association (Hergovich et al., 2005; Koike-Kumagai et al., 2009); thus, our findings that Raw is a membrane-associated protein, that Raw physically associates with Trc, and that the Raw TM-ICD mediates this interaction, suggested that Raw might play some role in Trc phosphorylation/activation.

To assess the functional relevance of the Raw-Trc interaction, we developed antibodies that allowed us to monitor Trc phosphorylation on threonine 449 (T449), the residue associated with maximal kinase activation (Fig. 6C; supplementary material Fig. S4) (Tamaskovic et al., 2003). First, we examined the relationship between Raw and Trc activation in S2 cells. In control or *GFP-raw*-transfected S2 cells, Trc P-T449 was present at low levels (Fig. 6D; for overexposed blot see supplementary material Fig. S4), suggesting that Raw is not sufficient to promote Trc phosphorylation. To examine whether Raw could facilitate Trc phosphorylation, we treated S2 cells with okadaic acid (OA) and monitored the effect of Raw on Trc P-T449 accumulation. As expected, OA treatment induced Trc phosphorylation (Koike-Kumagai et al., 2009; Millward et al., 1999), and Raw overexpression led to a 62% increase in OA-induced Trc phosphorylation (Fig. 6D). Thus, Raw can potentiate Trc activation in S2 cells. Further, the Raw TM-ICD was sufficient to potentiate Trc phosphorylation whereas the ECD exhibited no activity in this assay (Fig. 6E), suggesting that Raw enhances Trc phosphorylation by promoting Trc membrane association/proximity.

To examine whether Raw influences Trc activity *in vivo*, we assayed effects of *raw* mutation on Trc phosphorylation in C4da neurons. In the larval PNS, Trc P-T449 immunoreactivity was present at high levels in C4da dendrites, where it appeared to accumulate in puncta (Fig. 6F, $raw^{j102/+}$ heterozygote), consistent with prior reports that Trc is required for dendritic tiling in these neurons (Emoto et al., 2004). Trc P-T449 was also detectable in Class III da neurons, albeit at much lower levels, and *trc* is required for dendrite morphogenesis in these neurons as well (Fig. 6F, double arrowheads). Finally, Trc P-T449 was present at high levels in the axons of da neurons (Fig. 6F, bracket). By contrast, in *raw* mutant C4da MARCM clones, Trc P-T449 levels were substantially reduced to levels comparable to those in Class III da neurons (Fig. 6G). Thus, *raw* appears to potentiate Trc phosphorylation in C4da neurons as well as in S2 cells.

If *raw* functions through Trc to regulate dendrite-dendrite crossing, we reasoned that ectopic Trc activation in *raw* mutant neurons should mitigate the *raw* mutant dendrite crossing phenotype. This is indeed what we found. Although overexpressing wild-type Trc in *raw* mutant neurons had a dominant-negative effect (Fig. 6H,J), overexpression of myristoylated Trc, which is membrane targeted and hence constitutively active (Koike-Kumagai et al., 2009), significantly reduced dendrite-dendrite crossing in *raw* mutant neurons (Fig. 6I,J). Likewise, overexpression of a Trc phosphomimetic (*UAS-trc T449E*) partially suppressed the *raw* mutant dendrite-dendrite crossing defect (Fig. 6J). Thus, the *raw* mutant dendrite-dendrite crossing defect is likely to be caused, in part, by deficits in Trc activation, which Raw may potentiate by promoting Trc membrane association.

Trc can modulate dendrite adhesion to the ECM (Han et al., 2012); therefore, we investigated whether Raw can likewise modulate adhesion. We compared the adhesion of control or *GFP-raw*-expressing S2 cells to different ECM components (Fig. 7A). *GFP-raw* expression significantly enhanced S2 cell adhesion to collagen and, to a lesser degree, fibronectin (Fig. 7B). Since Raw can modulate Trc activity, and one output of Trc is cell adhesion (Han et al., 2012), we tested whether Raw promotes adhesion in a Trc-dependent manner. Indeed, a dominant-negative version of Trc (Trc K112A; Emoto et al., 2004) abrogated the ability of Raw to enhance adhesion to collagen (Fig. 7C).

Development (2015) 142, 162-173 doi:10.1242/dev.113423

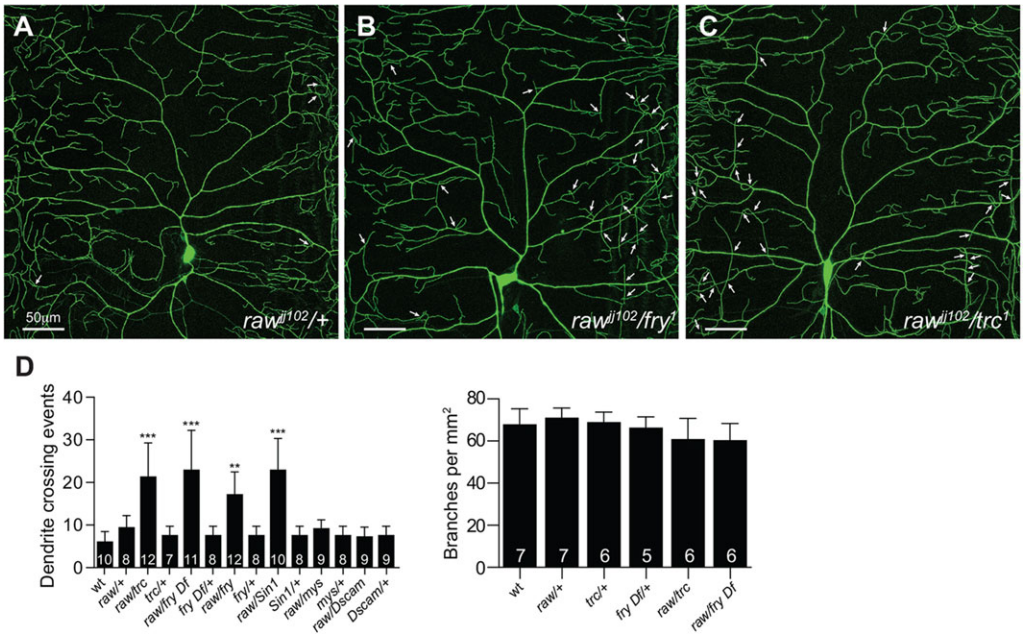

Fig. 5. Raw and Trc genetically interact. (A-C) C4da dendrites visualized using *pickpocket::mCD8-GFP* in raw^{ji102}/+ heterozygous (A) raw^{ji102}/fry^{1} double-heterozygous (B) and raw^{ji102}/trc^{1} double-heterozygous (C) larvae. (D) Quantification of dendrite crossing phenotypes and dendrite branch number. Error bars indicate s.d. $^{**}P<0.01$, $^{***}P<0.001$; one-way ANOVA with post-hoc Dunnett's test; number of neurons analyzed is indicated for each genotype.

Since Raw promotes S2 cell adhesion to collagen together with Trc, and Trc promotes Integrin-based attachment of C4da dendrites to a collagen-rich ECM (Han et al., 2012), we examined whether defects in Integrin-based adhesion contribute to the *raw* mutant dendrite phenotype. If *raw* modulates dendrite adhesion, we reasoned that increasing dendrite-ECM attachment should suppress the *raw* mutant dendrite-dendrite crossing defects, as Integrin overexpression suppresses dendrite-dendrite crossing defects of Trc pathway mutants (Han et al., 2012). To test this prediction, we assayed the effects of neuronal overexpression of Integrins (*UAS-mys+UAS-mew*) on terminal dendrite patterning in *raw* mutant C4da MARCM clones. Integrin overexpression suppressed dendrite-dendrite crossings in *raw* mutant neurons (Fig. 7F), suggesting that dendrite-ECM attachment is compromised in *raw* mutants, and significantly increased terminal branch number (Fig. 7G), which is likely to be the result of stabilizing the exuberant, short-lived branches found in *raw* mutant C4da neurons. Indeed, Integrin overexpression altered *raw* mutant terminal dendrite dynamics, increasing the fraction of stable terminals (Fig. 7H). However, Integrin overexpression did not rescue the *raw* mutant terminal dendrite elongation defect (Fig. 7I), suggesting that *raw* regulates branch stabilization and elongation via distinct mechanisms, with the former involving Trc.

Coordinate regulation of terminal dendrite adhesion and elongation by *raw*

Raw modulates F-actin assembly in cuticular hairs (Blake et al., 1999), and we noted that *raw* cell-autonomously regulated the formation of Actin-rich protrusions in oenocytes (supplementary material Fig. S5), suggesting that changes in Actin assembly might contribute to the dendrite extension defects of *raw* mutants. To investigate this possibility, we monitored F-actin distribution using GMA-GFP in wild-type and *raw* mutant C4da MARCM clones (supplementary material Fig. S6) (Bloor and Kiehart, 2001). In wild-type C4da dendrites, GMA-GFP was evenly distributed throughout the arbor with occasional concentrations at branch-points and in terminal dendrites. By contrast, terminal dendrites in *raw* mutant C4da neurons exhibited substantially higher levels of GMA-GFP than major dendrites. Thus, *raw* mutant terminal dendrites appear to be enriched in F-actin, which is likely to contribute to the dynamic behavior of these terminals. We examined whether Raw physically interacts with Actin or Tubulin, but we were unable to detect either Actin or Tubulin in Raw immunoprecipitates (data not shown). We also found that *raw* had little effect on the dendritic microtubule cytoskeleton visualized with Tubulin-GFP (supplementary material Fig. S6). Thus, we conclude that Raw indirectly regulates cytoskeletal composition to influence terminal dendrite elongation. Consistent with Raw regulating branch elongation independently of the *trc/fry* pathway, we did not observe GMA-GFP accumulation in terminal dendrites of *fry* mutants (supplementary material Fig. S7).

If indeed *raw* regulates terminal dendrite adhesion and elongation via distinct pathways, we reasoned that mutations in the signaling pathway(s) involved in branch elongation would selectively enhance the dendrite elongation phenotype of *raw* mutant neurons. To test this hypothesis, we screened our collection of terminal branching mutants for genetic interactions with *raw*. We identified one mutant (*jj472*) that genetically interacts with *raw* to affect terminal dendrite length and higher order branching without affecting the 3D orientation of terminal dendrites (Fig. 8A-C), further demonstrating that *raw* functions in terminal dendrite adhesion and elongation are genetically separable. Similar to *raw* mutant neurons, *raw jj472* double heterozygotes had shorter terminal dendrites and less complex terminal arbors; thus, the mean path length from the soma to branch endings was reduced in *raw jj472* double heterozygotes, as in *raw* mutant neurons (data not shown). On its own, homozygosity for *jj472* caused a significant decrease in terminal branch number and length, but only a modest increase in dendrite-dendrite crossing (Fig. 8D,E). *jj472* is loss-of-function allele of *AGO1*, which encodes an RNA-binding protein involved in miRNA-mediated translational repression (Förstemann et al., 2007; Kataoka et al., 2001), as *jj472* fails to complement $AGO1^{k00208}$ and $AGO1^{k08121}$. *jj472* carries a premature stop codon (Q319Stop) that truncates AGO1 before the catalytic domain (Hock and Meister, 2008), and *AGO1* RNAi and $AGO1^{k08121}$ phenocopy the dendrite defects of *jj472* (Fig. 8F,G; data not shown).

Altogether, our results support a model in which *raw* regulates terminal dendrite adhesion/stability and elongation by distinct

Development (2015) 142, 162-173 doi:10.1242/dev.113423

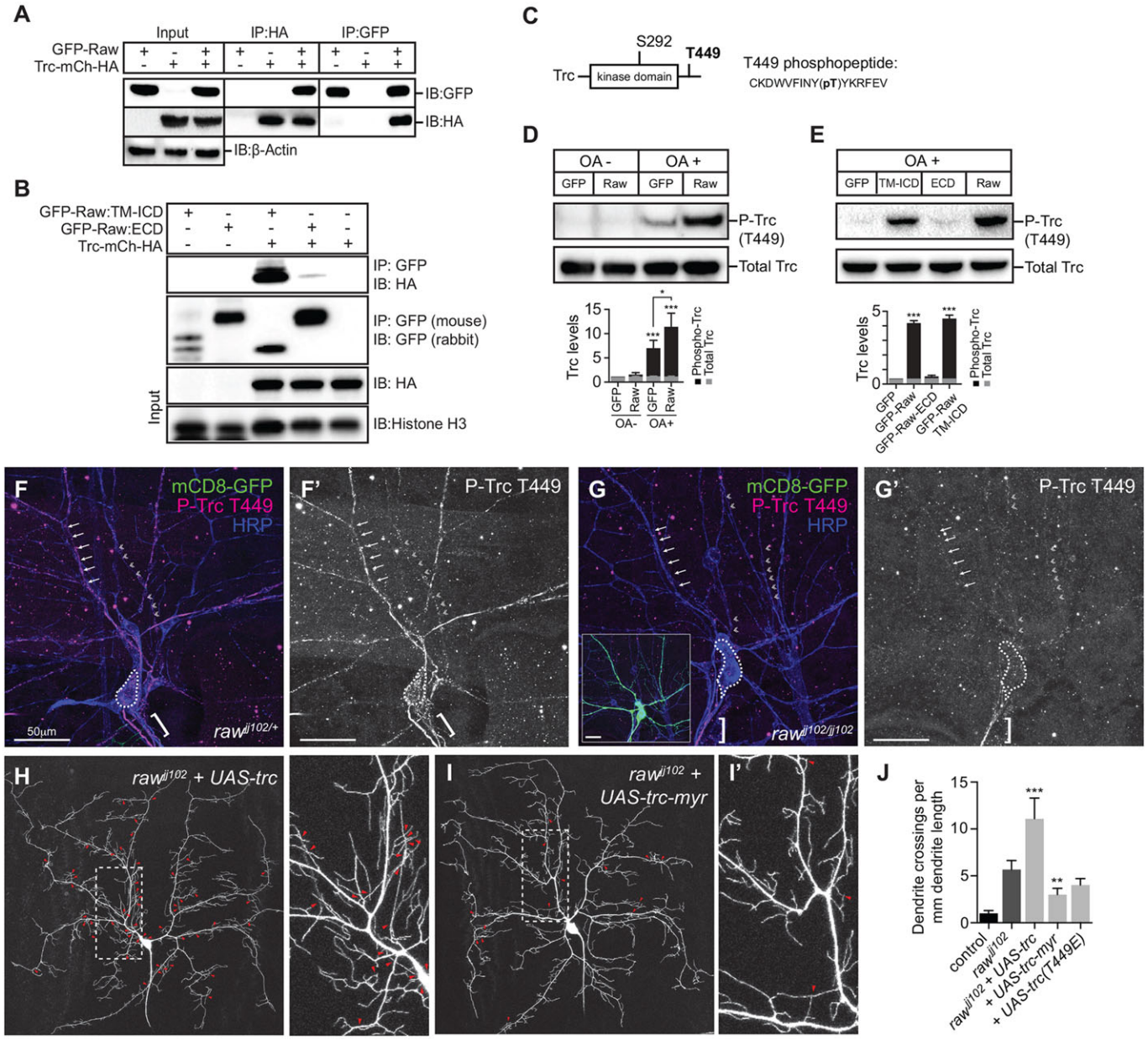

Fig. 6. Raw promotes Trc activation. (A,B) Raw-Trc association. Lysates of S2 cells transfected with *Trc-mCherry-HA* and/or (A) *GFP-raw* and (B) *GFP-raw:TM-ICD* or *GFP-raw:ECD* were immunoprecipitated (IP) and immunoblotted (IB) with the indicated antibodies. Loading controls were provided by β-Actin (A) and Histone H3 (B). (C-E) Raw potentiates Trc phosphorylation. (C) Trc schematic depicting phosphorylation sites (left), and the phosphoepitope used to generate Trc P-T449 antibodies (right). (D) S2 cells were transfected with *GFP* or *GFP-raw* and Trc phosphorylation on T449 was assayed in the absence or presence of okadaic acid (OA) treatment using phospho-specific antibodies (see also supplementary material Fig. S2). Bar chart shows the mean levels (four independent experiments) of total Trc and phospho-Trc in cell lysates. (E) The Raw TM-ICD fragment but not the ECD fragment potentiates Trc phosphorylation. (F-G′) Raw promotes Trc phosphorylation in C4da neurons. Immunostaining in raw^{ji102}/+ larvae carrying C4da raw^{ji102} raw^{ji102} MARCM clones. Phospho-Trc (P-T449) immunoreactivity (magenta), anti-HRP to label sensory neurons (blue) and anti-GFP to label MARCM clones (inset, G) are shown. White dotted lines outline C4da cell bodies; brackets mark axons. Arrows indicate C4da dendrites; double-chevrons mark C3da dendrites. (H-J) Raw promotes Trc activation to regulate dendrite-dendrite crossing. *UAS-trc* (H), *UAS-trc-myr* (I) or *UAS-trc T449E* (J) was expressed in raw^{ji102} C4da MARCM clones and effects on dendrite-dendrite crossing were analyzed (J). Red arrowheads indicate dendrite-dendrite crossings. ***P*<0.01, ****P*<0.001; one-way ANOVA with post-hoc Dunnett's test. Error bars indicate s.d.

pathways (Fig. 8J). Knockdown of one of these pathways causes terminal dendrite elongation defects (*AGO1-RNAi*, Fig. 8G) or dendrite-dendrite crossing defects (*trc-RNAi*, Fig. 8H), whereas knockdown of both pathways has an additive effect, resulting in dendrite defects similar to those of *raw* mutants (Fig. 8I). We have not yet characterized the *raw-AGO1* interaction in detail, as *AGO1* overexpression causes severe patterning defects and occasional neuron death, and we have been unable to generate double-mutant MARCM clones, so their respective functions in dendrite elongation remain to be determined. One possibility is that Raw interacts with AGO1 to influence the local translation of key effectors of terminal dendrite growth, as miRNAs are known to regulate local translation in dendrites in some neurons (Vo et al., 2010) and several factors with roles in local translation affect terminal dendrite growth in C4da neurons (Olesnicky et al., 2014).

Development (2015) 142, 162-173 doi:10.1242/dev.113423

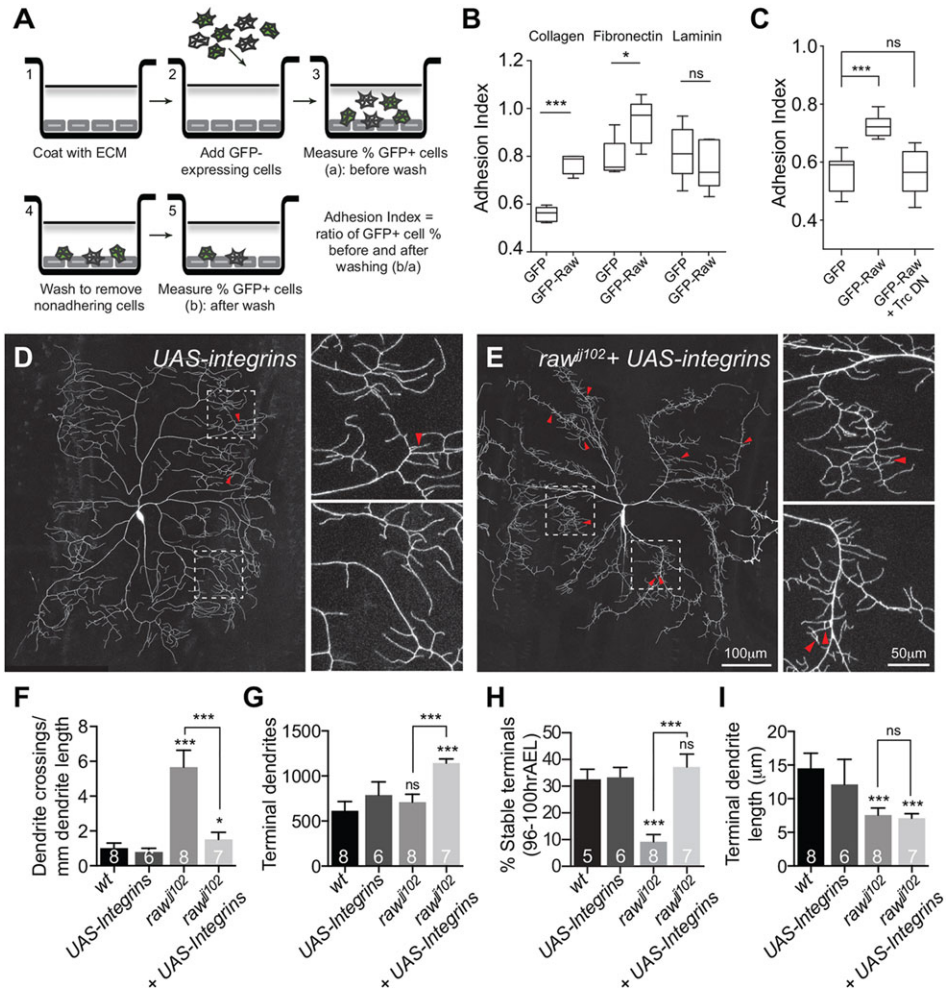

Fig. 7. Raw modulates cell adhesion. (A) S2 cell adhesion assay. (B) Cell adhesion to different substrates. S2 cells were transfected with *Actin-Gal4+UAS-GFP* or *UAS-GFP-raw*, and adhesion was assayed 2 days post-transfection. (C) Cell adhesion to collagen was measured as in B, but cells were additionally co-transfected with a dominant-negative version of Trc (*Trc-DN; UAS-trc K112A*). Box plots depict mean values and first/third quartile from five experiments (>100 cells scored for each experiment); whiskers denote maximum/minimum values. ns, not significant; **P*<0.05, ****P*<0.001, compared with *Actin-Gal4+UAS-GFP*-transfected S2 cells; Student's *t*-test in B, one-way ANOVA with a post-hoc Dunnett's test in C. (D-G) Integrin-based adhesion promotes terminal dendrite stability. (D,E) Overexpression of Integrins (*UAS-mys+UAS-mew*) in a control (D) or *raw*^{ij102} (E) C4da neuron. Arrowheads indicate dendrite-dendrite crossings. (F-I) Quantification of terminal dendrite crossings (F), number (G), dynamics (H) and length (I) in the indicated genotypes. The number of neurons analyzed for each genotype is indicated within each bar. ns, not significant; **P*<0.05, ****P*<0.001, compared with *UAS-Integrins*; one-way ANOVA with post-hoc Dunnett's test. Error bars indicate s.d.

DISCUSSION

Although the concept of positional information was first applied to embryonic development (Wolpert, 1969), intracellular positional information governs morphogenesis of individual cells as well. For example, positioning the nucleus at the cell center and growth zones at the cell periphery depends on positional information from the microtubule cytoskeleton in *Schizosaccharomyces pombe* (Bähler and Pringle, 1998; Castagnetti et al., 2007; Hagan and Yanagida, 1997). Several lines of evidence support the existence of distinct subcompartments in axons and dendrites, but the forms of intracellular positional information and the coordinate systems that guide the development of these subcompartments have not been extensively characterized. Results from our screen and other studies suggest that at least two types of positional information govern C4da dendrite patterning. First, terminal branch distribution along the proximal-distal axis depends on microtubule-based processes; perturbing microtubule-based transport leads to a distal-proximal shift in the distribution of terminal dendrites in C4da arbors (Satoh et al., 2008; Zheng et al., 2008). Interestingly, modulating the activity of the F-actin nucleator Spire also affects terminal dendrite positioning along the proximal-distal axis (Ferreira et al., 2014), suggesting that multiple pathways contribute to the fidelity of branch placement. Second, terminal dendrites rely on dedicated programs that may act locally to regulate terminal dendrite patterning. Our observation that different pathways regulate different aspects of terminal dendrite development suggests that multiple signaling systems exist for the local control of dendrite growth.

We identified *raw* as a key regulator of terminal dendrite patterning. *raw* encodes a membrane protein that accumulates at branch-points and coordinately regulates terminal dendrite adhesion/stability via a pathway that involves Trc and terminal dendrite elongation via a pathway that is likely to involve cytoskeletal remodeling and AGO1. Raw therefore provides a potential point of integration for external signals that regulate these downstream growth programs. These pathways could be responsive to the same signal – for example, Raw association with an extracellular ligand or a co-receptor – or could be spatially/sequentially segregated. Identification of additional *raw*-interacting genes should help clarify the architecture of these signaling pathways.

Raw regulates cell-cell signaling (Bates et al., 2008; Bauer Huang et al., 2007; Byars et al., 1999; Jemc et al., 2012), and in gonad morphogenesis Raw modulates Cadherin-based interactions between somatic gonadal precursor cells and germ cells, in part by localizing Armadillo to the cell surface (Jemc et al., 2012). Likewise, our data support a role for Raw in promoting Trc activation by localizing Trc to the plasma membrane. Thus, one plausible model for Raw function in dendrite development is that it interacts with an extracellular signal, which might be a component of the ECM or a cell surface protein on epithelial cells, and signals together with a co-receptor to stimulate downstream pathways for adhesion and cytoskeletal remodeling. Several analogous signaling systems involving interactions with the epidermis that influence terminal dendrite or sensory axon patterning have been described (Chiang et al., 2011; Dong et al., 2013; Han et al., 2012; Kim et al.,

Development (2015) 142, 162-173 doi:10.1242/dev.113423

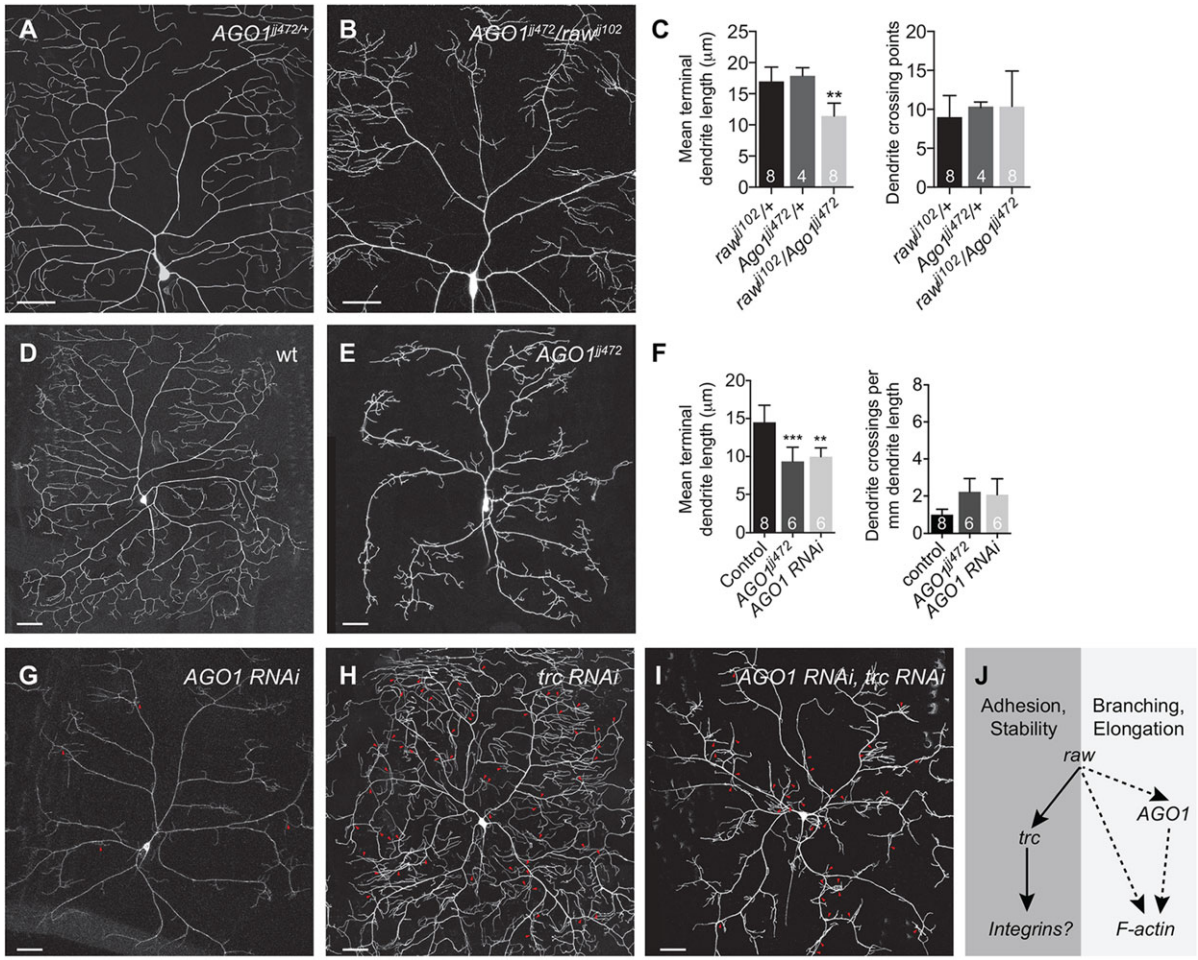

Fig. 8. Coordinate control of terminal dendrite adhesion and elongation by *raw*. (A-C) *AGO1* and *raw* genetically interact to regulate terminal dendrite length. Representative images of C4da neurons (*ppk-mCD8-GFP*) are shown for $AGO1^{ij472}$/+ (A) and $AGO1^{ij472}/raw^{ij102}$ (B) heterozygotes. (C) Mean terminal dendrite length (left) and average number of dendrite crossing points (right) in larvae of the indicated genotypes. The number of C4da neurons analyzed for each genotype is indicated within each bar. (D-F) *AGO1* regulates terminal dendrite growth. Representative C4da MARCM clones shown for wild-type control (D) and $AGO1^{ij472}$ (E). (F) Mean terminal dendrite length (left) and crossing points (right) for the indicated genotypes. $^{**}P<0.01$, $^{***}P<0.001$; one-way ANOVA with post-hoc Dunnett's test. (G-I) Additive effects of *trc* and *AGO1* knockdown on dendrite patterning. (G) *UAS-AGO1-RNAi*, (H) *UAS-trc-RNAi* or (I) *UAS-AGO1-RNAi+UAS-trc-RNAi*. Arrowheads indicate dendrite-dendrite crossing points. (J) Genetic pathway for *raw* control of terminal dendrite patterning. Raw independently regulates terminal dendrite adhesion/stability and branching/branch elongation. *raw* functions upstream of *trc* to promote terminal dendrite adhesion and stability, perhaps via integrins. *raw* regulates terminal branching and branch elongation via a pathway that involves *AGO1* and *F-actin* assembly, but the position and relative contribution of each component in this pathway is unknown, hence the dashed lines. Error bars indicate s.d. Scale bars: 50 μm.

2012; Salzberg et al., 2013), but how many of these signaling systems are at work in a given neuron, and how Raw interfaces with other signaling pathways, remain to be determined.

Although Raw has no obvious vertebrate counterpart, stretches of the ECD bear similarity to mucins and leucine-rich repeat proteins, one of which might serve an analogous function. Moreover, components of both downstream signaling pathways that we identified are conserved in vertebrates and play known roles in dendrite patterning, including roles in the local control of dendrite growth: the Trc orthologs NDR1/2 (STK38/STK38L) regulate aspects of dendrite branch and spine morphogenesis (Ultanir et al., 2012), and Argonaute proteins mediate miRNA-mediated control of dendrite patterning, in part through local effects on translation (Vo et al., 2010). Additionally, dendrites contain structures related to P-granules, and Argonaute proteins may influence local translation in P-granules as well (Cougot et al., 2008). Thus, versions of the Raw-regulated signaling pathways might control terminal dendrite patterning in vertebrates.

MATERIALS AND METHODS

Fly stocks

A list of alleles used in this study and details of the genetic screen are provided in supplementary material methods and Table S1.

Live imaging

Imaging was performed as described (Jiang et al., 2014). For time-lapse analysis, larvae were imaged at the indicated time, recovered to yeasted agar plates with vented lids, aged at 25°C, and imaged again.

Immunohistochemistry

Larval fillets were dissected and processed as described (Grueber et al., 2002) and stained with HRP conjugated with Cy5 (1:250; 123-175-021, Jackson ImmunoResearch), anti-mCD8 (1:100; MCD0800, Life Technologies), anti-GFP (1:500; A11122, Life Technologies), anti-β-gal (1:500; A11132, Life Technologies), anti-Trc-P-T449 (1:500; this study), and secondary antibodies from Jackson ImmunoResearch (112-225-003, 111-295-144; 1:250).

Development (2015) 142, 162-173 doi:10.1242/dev.113423

Phospho-Trc antibody

Antibodies from rabbits immunized with a KLH-conjugated phosphorylated peptide (CKDWVFINY-pT-YKRFE) were affinity purified with bead-conjugated phospho-peptide. Non-phospho-specific antibodies were removed by absorption against a non-phosphorylated version of the antigen (Yenzym). In Trc phosphorylation assays, total Trc levels were assessed with anti-Trc antibodies [1:1000; courtesy of K. Emoto; Koike-Kumagai et al. (2009)] and protein input was assessed with anti-Actin (1:5000; ab8224, Abcam) or anti-Histone H3 (1:2000; H0164, Sigma) antibodies.

Surface staining

Formaldehyde (4%) fixed fillets were washed/stained without detergent to prevent permeabilization. Rhodamine-conjugated secondary antibodies (1:250; 123-175-021; Jackson Immunoresearch) were used for surface staining to ensure that surface-exposed GFP could be differentiated from total GFP.

Cell culture

S2 cells were grown as described (Rogers and Rogers, 2008), transfected using Effectene (Qiagen), and treated with 100 nM okadaic acid (Sigma) for 30 min before harvesting, where indicated.

Immunoprecipitations

Two days post-transfection, cells were lysed in NP-40 buffer. One milligram of extract was incubated with primary antibodies to GFP (2 µg; A11120, Life Technologies) or HA (2 µg; 11867431001, Roche) for 2 h, followed by Protein-G Agarose (Roche) for 1 h. Beads were washed five times in lysis buffer and bound proteins were analyzed by SDS-PAGE and western blotting with antibodies to GFP (1:500; A11122, Life Technologies) or HA (1:2000; 11867431001, Roche).

Cell adhesion assay

Transfected S2 cells were plated for 1 h in a 6-well cell culture plate coated with collagen I, fibronectin, or laminin (Life Technologies). Cells were washed twice with PBS and counted in four fields of view, then washed three time with PBS and counted as before, from which we calculated an adhesion index as the ratio of GFP-positive cells before/after washing.

Cell fractionation

Transfected S2 cells were lysed in fractionation buffer [250 mM sucrose, 20 mM HEPES pH 7.4, 10 mM KCl, 1.5 mM $MgCl_2$, 1 mM EDTA, 1 mM EGTA, 1 mM DTT, Complete protease inhibitor (Life Technologies)] with Dounce homogenization. Lysates were fractionated by centrifugation: 720 ***g*** for 5 minutes (nuclear), 10,000 ***g*** 5 for minutes (mitochondria) and 100,000 ***g*** for 1 h for membrane (pellet) and cytosolic (soluble) fractions. Fractions were analyzed by SDS-PAGE and western blotting with antibodies against GFP (1:500; A11122, Life Technologies), Robo and Tubulin (13C9 at 1:200, 12G10 at 1:2000, respectively; both from Developmental Studies Hybridoma Bank).

Molecular biology

Raw-short was PCR amplified from cDNA clone GH23250 (*Drosophila* Genomics Resource Center, Bloomington, IN, USA) and cloned into pUAST (Drosophila Genomics Resource Center) with N-terminal EGFP derived from pEGFP-N1 (Clontech). Transgenics services were provided by BestGene.

Dendrite measurements

Dendrite length, crossing and dynamics were analyzed as described previously (Jiang et al., 2014); for details, see supplementary material methods.

Statistical analysis

Differences between group means were analyzed by ANOVA with a post-hoc Dunnett's test; pairwise comparisons of group means were performed with Student's *t*-test. Binomial tests were used to evaluate whether terminal dynamics differed between control and *raw* mutant neurons (Fig. 2D). Chi-squared tests were used to evaluate whether the presence/absence of GFP-Raw at branch-points influenced terminal dynamics (Fig. 3C).

Acknowledgements

We thank the Bloomington Stock Center, Giovanni Bosco, Simon Collier, Kazuo Emoto, Eric Lai, Anthea Letsou, Peter Soba and Tadashi Uemura for fly stocks; Kazuo Emoto and the Developmental Studies Hybridoma Bank for antibodies; the Drosophila Genomics Resource Center for cDNA clones; Ashley Lau and Hannah Lampert for screening and stereology assistance; David Parichy, Michael Kim and Peter Soba for critical reading of the manuscript.

Competing interests

The authors declare no competing financial interests.

Author contributions

J.L. and J.Z.P. designed the experiments. Y.P. constructed truncated *UAS-raw* transgenes and performed cell adhesion assays. W.Y.L. constructed *UAS-raw* transgenes. J.L. and J.Z.P. conducted all other experiments. J.L. and J.Z.P. analyzed the data and wrote the manuscript.

Funding

This work was supported by the National Institutes of Health [NIMH R00-MH084277, NINDS R01-NS076614], a March of Dimes Basil O'Connor Award, a Klingenstein Fellowship in Neuroscience (J.Z.P.) and a Benjamin Hall Fellowship (J.L.). Deposited in PMC for release after 12 months.

Supplementary material

Supplementary material available online at
http://dev.biologists.org/lookup/suppl/doi:10.1242/dev.113423/-/DC1

References

Aridor, M., Guzik, A. K., Bielli, A. and Fish, K. N. (2004). Endoplasmic reticulum export site formation and function in dendrites. *J. Neurosci.* **24**, 3770-3776.

Baas, P. W., Deitch, J. S., Black, M. M. and Banker, G. A. (1988). Polarity orientation of microtubules in hippocampal neurons: uniformity in the axon and nonuniformity in the dendrite. *Proc. Natl. Acad. Sci. USA* **85**, 8335-8339.

Bähler, J. and Pringle, J. R. (1998). Pom1p, a fission yeast protein kinase that provides positional information for both polarized growth and cytokinesis. *Genes Dev.* **12**, 1356-1370.

Bates, K. L., Higley, M. and Letsou, A. (2008). Raw mediates antagonism of AP-1 activity in Drosophila. *Genetics* **178**, 1989-2002.

Bauer Huang, S. L., Saheki, Y., VanHoven, M. K., Torayama, I., Ishihara, T., Katsura, I., van der Linden, A., Sengupta, P. and Bargmann, C. I. (2007). Left-right olfactory asymmetry results from antagonistic functions of voltage-activated calcium channels and the Raw repeat protein OLRN-1 in C. elegans. *Neural Dev.* **2**, 24.

Blake, K. J., Myette, G. and Jack, J. (1999). ribbon, raw, and zipper have distinct functions in reshaping the Drosophila cytoskeleton. *Dev. Genes Evol.* **209**, 555-559.

Bloor, J. W. and Kiehart, D. P. (2001). zipper Nonmuscle Myosin-II functions downstream of PS2 Integrin in Drosophila Myogenesis and is necessary for Myofibril formation. *Dev. Biol.* **239**, 215-228.

Byars, C. L., Bates, K. L. and Letsou, A. (1999). The dorsal-open group gene raw is required for restricted DJNK signaling during closure. *Development* **126**, 4913-4923.

Castagnetti, S., Novák, B. and Nurse, P. (2007). Microtubules offset growth site from the cell centre in fission yeast. *J. Cell Sci.* **120**, 2205-2213.

Chatterjee, N. and Bohmann, D. (2012). A versatile ΦC31 based reporter system for measuring AP-1 and Nrf2 signaling in Drosophila and in tissue culture. *PLoS ONE* **7**, e34063.

Chen, Y. and Sabatini, B. L. (2012). Signaling in dendritic spines and spine microdomains. *Curr. Opin. Neurobiol.* **22**, 389-396.

Chiang, L.-Y., Poole, K., Oliveira, B. E., Duarte, N., Sierra, Y. A. B., Bruckner-Tuderman, L., Koch, M., Hu, J. and Lewin, G. R. (2011). Laminin-332 coordinates mechanotransduction and growth cone bifurcation in sensory neurons. *Nat. Neurosci.* **14**, 993-1000.

Cougot, N., Bhattacharyya, S. N., Tapia-Arancibia, L., Bordonné, R., Filipowicz, W., Bertrand, E. and Rage, F. (2008). Dendrites of mammalian neurons contain specialized P-body-like structures that respond to neuronal activation. *J. Neurosci.* **28**, 13793-13804.

Dong, X., Liu, O. W., Howell, A. S. and Shen, K. (2013). An extracellular adhesion molecule complex patterns dendritic branching and morphogenesis. *Cell* **155**, 296-307.

Emoto, K., He, Y., Ye, B., Grueber, W. B., Adler, P. N., Jan, L. Y. and Jan, Y.-N. (2004). Control of dendritic branching and tiling by the Tricornered-kinase/Furry signaling pathway in Drosophila sensory neurons. *Cell* **119**, 245-256.

Ferreira, T., Ou, Y., Li, S., Giniger, E. and van Meyel, D. J. (2014). Dendrite architecture organized by transcriptional control of the F-actin nucleator Spire. *Development* **141**, 650-660.

Förstemann, K., Horwich, M. D., Wee, L., Tomari, Y. and Zamore, P. D. (2007). Drosophila microRNAs are sorted into functionally distinct argonaute complexes after production by dicer-1. *Cell* **130**, 287-297.
Fujishima, K., Horie, R., Mochizuki, A. and Kengaku, M. (2012). Principles of branch dynamics governing shape characteristics of cerebellar Purkinje cell dendrites. *Development* **139**, 3442-3455.
Gardiol, A., Racca, C. and Triller, A. (1999). Dendritic and postsynaptic protein synthetic machinery. *J. Neurosci.* **19**, 168-179.
Gavrikov, K. E., Nilson, J. E., Dmitriev, A. V., Zucker, C. L. and Mangel, S. C. (2006). Dendritic compartmentalization of chloride cotransporters underlies directional responses of starburst amacrine cells in retina. *Proc. Natl. Acad. Sci. USA* **103**, 18793-18798.
Grueber, W. B., Jan, L. Y. and Jan, Y. N. (2002). Tiling of the Drosophila epidermis by multidendritic sensory neurons. *Development* **129**, 2867-2878.
Hagan, I. and Yanagida, M. (1997). Evidence for cell cycle-specific, spindle pole body-mediated, nuclear positioning in the fission yeast Schizosaccharomyces pombe. *J. Cell Sci.* **110**, 1851-1866.
Han, C., Wang, D., Soba, P., Zhu, S., Lin, X., Jan, L. Y. and Jan, Y.-N. (2012). Integrins regulate repulsion-mediated dendritic patterning of drosophila sensory neurons by restricting dendrites in a 2D space. *Neuron* **73**, 64-78.
Hergovich, A., Bichsel, S. J. and Hemmings, B. A. (2005). Human NDR kinases are rapidly activated by MOB proteins through recruitment to the plasma membrane and phosphorylation. *Mol. Cell. Biol.* **25**, 8259-8272.
Höck, J. and Meister, G. (2008). The Argonaute protein family. *Genome Biol.* **9**, 210.
Horton, A. C. and Ehlers, M. D. (2003). Dual modes of endoplasmic reticulum-to-Golgi transport in dendrites revealed by live-cell imaging. *J. Neurosci.* **23**, 6188-6199.
Imamura, F. and Greer, C. A. (2009). Dendritic branching of olfactory bulb mitral and tufted cells: regulation by TrkB. *PLoS ONE* **4**, e6729.
Jack, J. and Myette, G. (1997). The genes raw and ribbon are required for proper shape of tubular epithelial tissues in Drosophila. *Genetics* **147**, 243-253.
Jemc, J. C., Milutinovich, A. B., Weyers, J. J., Takeda, Y. and Van Doren, M. (2012). raw Functions through JNK signaling and cadherin-based adhesion to regulate Drosophila gonad morphogenesis. *Dev. Biol.* **367**, 114-125.
Jiang, N., Soba, P., Parker, E., Kim, C. C. and Parrish, J. Z. (2014). The microRNA bantam regulates a developmental transition in epithelial cells that restricts sensory dendrite growth. *Development* **141**, 2657-2668.
Jinushi-Nakao, S., Arvind, R., Amikura, R., Kinameri, E., Liu, A. W. and Moore, A. W. (2007). Knot/Collier and cut control different aspects of dendrite cytoskeleton and synergize to define final arbor shape. *Neuron* **56**, 963-978.
Jones, D. T., Taylor, W. R. and Thornton, J. M. (1994). A model recognition approach to the prediction of all-helical membrane protein structure and topology. *Biochemistry* **33**, 3038-3049.
Kania, A., Salzberg, A., Bhat, M., D'Evelyn, D., He, Y., Kiss, I. and Bellen, H. J. (1995). P-element mutations affecting embryonic peripheral nervous system development in Drosophila melanogaster. *Genetics* **139**, 1663-1678.
Kataoka, Y., Takeichi, M. and Uemura, T. (2001). Developmental roles and molecular characterization of a Drosophila homologue of Arabidopsis Argonaute1, the founder of a novel gene superfamily. *Genes Cells* **6**, 313-325.
Katsuki, T., Joshi, R., Ailani, D. and Hiromi, Y. (2011). Compartmentalization within neurites: its mechanisms and implications. *Dev. Neurobiol.* **71**, 458-473.
Kim, M. E., Shrestha, B. R., Blazeski, R., Mason, C. A. and Grueber, W. B. (2012). Integrins establish dendrite-substrate relationships that promote dendritic self-avoidance and patterning in drosophila sensory neurons. *Neuron* **73**, 79-91.
Koike-Kumagai, M., Yasunaga, K.-i., Morikawa, R., Kanamori, T. and Emoto, K. (2009). The target of rapamycin complex 2 controls dendritic tiling of Drosophila sensory neurons through the Tricornered kinase signalling pathway. *EMBO J.* **28**, 3879-3892.
Lee, T. and Luo, L. (1999). Mosaic analysis with a repressible cell marker for studies of gene function in neuronal morphogenesis. *Neuron* **22**, 451-461.
Long, H., Ou, Y., Rao, Y. and van Meyel, D. J. (2009). Dendrite branching and self-avoidance are controlled by Turtle, a conserved IgSF protein in Drosophila. *Development* **136**, 3475-3484.
Masland, R. H. (2004). Neuronal cell types. *Curr. Biol.* **14**, R497-R500.
Matthews, B. J., Kim, M. E., Flanagan, J. J., Hattori, D., Clemens, J. C., Zipursky, S. L. and Grueber, W. B. (2007). Dendrite self-avoidance is controlled by Dscam. *Cell* **129**, 593-604.
Millward, T. A., Hess, D. and Hemmings, B. A. (1999). Ndr protein kinase is regulated by phosphorylation on two conserved sequence motifs. *J. Biol. Chem.* **274**, 33847-33850.
Nüsslein-Volhard, C., Wieschaus, E. and Kluding, H. (1984). Mutations affecting the pattern of the larval cuticle in Drosophila melanogaster. *Rouxs Arch. Dev. Biol.* **193**, 267-282.
Olesnicky, E. C., Killian, D. J., Garcia, E., Morton, M. C., Rathjen, A. R., Sola, I. E. and Gavis, E. R. (2014). Extensive use of RNA-binding proteins in Drosophila sensory neuron dendrite morphogenesis. *G3 (Bethesda)* **4**, 297-306.
Parrish, J. Z., Kim, M. D., Jan, L. Y. and Jan, Y. N. (2006). Genome-wide analyses identify transcription factors required for proper morphogenesis of Drosophila sensory neuron dendrites. *Genes Dev.* **20**, 820-835.
Parrish, J. Z., Xu, P., Kim, C. C., Jan, L. Y. and Jan, Y. N. (2009). The microRNA bantam functions in epithelial cells to regulate scaling growth of dendrite arbors in drosophila sensory neurons. *Neuron* **63**, 788-802.
Prokopenko, S. N., He, Y., Lu, Y. and Bellen, H. J. (2000). Mutations affecting the development of the peripheral nervous system in Drosophila: a molecular screen for novel proteins. *Genetics* **156**, 1691-1715.
Rogers, S. L. and Rogers, G. C. (2008). Culture of Drosophila S2 cells and their use for RNAi-mediated loss-of-function studies and immunofluorescence microscopy. *Nat. Protoc.* **3**, 606-611.
Salzberg, Y., Díaz-Balzac, C. A., Ramirez-Suarez, N. J., Attreed, M., Tecle, E., Desbois, M., Kaprielian, Z. and Bülow, H. E. (2013). Skin-derived cues control arborization of sensory dendrites in Caenorhabditis elegans. *Cell* **155**, 308-320.
Satoh, D., Sato, D., Tsuyama, T., Saito, M., Ohkura, H., Rolls, M. M., Ishikawa, F. and Uemura, T. (2008). Spatial control of branching within dendritic arbors by dynein-dependent transport of Rab5-endosomes. *Nat. Cell Biol.* **10**, 1164-1171.
Soba, P., Zhu, S., Emoto, K., Younger, S., Yang, S.-J., Yu, H.-H., Lee, T., Jan, L. Y. and Jan, Y.-N. (2007). Drosophila sensory neurons require Dscam for dendritic self-avoidance and proper dendritic field organization. *Neuron* **54**, 403-416.
Tamaskovic, R., Bichsel, S. J., Rogniaux, H., Stegert, M. R. and Hemmings, B. A. (2003). Mechanism of Ca2+-mediated regulation of NDR protein kinase through autophosphorylation and phosphorylation by an upstream kinase. *J. Biol. Chem.* **278**, 6710-6718.
Ultanir, S. K., Hertz, N. T., Li, G., Ge, W.-P., Burlingame, A. L., Pleasure, S. J., Shokat, K. M., Jan, L. Y. and Jan, Y.-N. (2012). Chemical genetic identification of NDR1/2 kinase substrates AAK1 and Rabin8 Uncovers their roles in dendrite arborization and spine development. *Neuron* **73**, 1127-1142.
Vo, N. K., Cambronne, X. A. and Goodman, R. H. (2010). MicroRNA pathways in neural development and plasticity. *Curr. Opin. Neurobiol.* **20**, 457-465.
Wolpert, L. (1969). Positional information and the spatial pattern of cellular differentiation. *J. Theor. Biol.* **25**, 1-47.
Ye, B., Zhang, Y., Song, W., Younger, S. H., Jan, L. Y. and Jan, Y. N. (2007). Growing dendrites and axons differ in their reliance on the secretory pathway. *Cell* **130**, 717-729.
Yuste, R. (2013). Electrical compartmentalization in dendritic spines. *Annu. Rev. Neurosci.* **36**, 429-449.
Zheng, Y., Wildonger, J., Ye, B., Zhang, Y., Kita, A., Younger, S. H., Zimmerman, S., Jan, L. Y. and Jan, Y. N. (2008). Dynein is required for polarized dendritic transport and uniform microtubule orientation in axons. *Nat. Cell Biol.* **10**, 1172-1180.